Smart design for CBRN protection by coupling adsorption and photocatalysis: Regeneration adsorbent efficiency-CWAs' continuous purification

Youcef Serhane, Abdelkrim Bouzaza, Dominique Wolbert, Amina Meslem, Aymen Amin Assadi

To cite this version:

Youcef Serhane, Abdelkrim Bouzaza, Dominique Wolbert, Amina Meslem, Aymen Amin Assadi. Smart design for CBRN protection by coupling adsorption and photocatalysis: Regeneration adsorbent efficiency-CWAs' continuous purification. Chemical Engineering Journal, 2023, 471, pp.144326. 10.1016/j.cej.2023.144326 . hal-04193513

HAL Id: hal-04193513
https://hal.science/hal-04193513
Submitted on 4 Sep 2024

Smart Design for CBRN Protection by Coupling Adsorption and Photocatalysis: Regeneration Adsorbent Efficiency – CWAs' Continuous Purification

Youcef Serhane[a], Abdelkrim Bouzaza[a], Dominique Wolbert[a], Amina Meslem[b], Aymen Amin Assadi[a,*]

[a] Univ Rennes, École Nationale Supérieure de Chimie de Rennes, CNRS, ISCR (Institut des Sciences Chimiques de Rennes) – UMR 6226, F-35000 Rennes, France

[b] Univ Rennes, LGCGM, 3 Rue du Clos Courtel, BP 90422, 35704, Rennes, CEDEX 7, France

*Corresponding author. Tel: +33(0)223238152, Fax: +33(0)223238120,

E-mail: Aymen.assadi@ensc-rennes.fr

ABSTRACT

This investigation and optimization of the adsorption and photocatalysis coupling process for treating chemical warfare agents (CWAs) were performed with a compact cartridge based on activated carbon felt (AF) and TiO_2 photocatalyst deposited on luminous textiles. The target pollutants were simulants of the chemical warfare agent (yperite), methyl salicylate, diethyl sulfur (a simulant of sulfur mustard gas), and cyclohexane, which is the benchmark for type A gas filtration tests. To take better advantage of this new configuration, an optimization of the photocatalytic process was highlighted with an improvement of the regeneration process by implementing the integrated compactness of desorption by the Joule effect (*in situ*). In the case of methyl salicylate treatment, the recovery of the adsorption capacity of the AF were about 95% and a working time of 85% compared to initial adsorbent performance. For the second cycle regeneration, the recovered adsorption capacity was about 88%

compared to initial capacity. We note also that the working time decrease by 15% for each regeneration step. The evaluation of the new coupling configuration aimed at highlighting the influence of a sulfur compound was encouraging, with a regeneration rate of the adsorbent of about 80%. Compared to MS, the regeneration seems to be more difficult. This is due to by-products (SO_2, MSH) formation which is highlighted by the degradation pathway proposed. The removal efficiency of the coupling system (UV-LED/AF) under continuous process, was equal to 36%. This leads an increase in filter working time of 50 min over that of a conventional adsorption process. Special attention was paid to validating the coupling system performance in real conditions. The system was placed on a humanlike seated thermal manikin used to simulate an occupant of a chamber of 30 m^3 with the realistic condition of applying chemical, biological, radiological, and nuclear (CBRN) agent protection. The time protection was 60 and 30 min for respective concentrations of about 150 and 300 $mg.m^{-3}$.

This global investigation addressed how to overcome the scientific barriers to designing a compact, self-contained filtration cartridge for personal protection in CBRN emergency response and management in accordance with the United Nations Sustainable Development Goals (SDGs).

Keywords

chemical weapon agent’s treatment, optimized coupling photocatalytic/adsorption configuration; regeneration; CBRN emergency.

1. Introduction

To fight against chemical weapons, government authorities have conducted several actions, either at the international level through a commitment to the Organization for the Prohibition of Chemical Weapons (OPCW) and through the implementation of the

Convention on the Prohibition of the Development, Production, Stockpiling and Use of Chemical Weapons and on Their Destruction [1]. or at the national level through the elaboration of defense strategies (e.g., plans, laws, and treaties). These application have prepared personnel to improve their capacity to act and their research and development, in particular, for developing new processes for treating chemical warfare agents, which has become the main subject of study for researchers [2][3][4]. Chemical warfare agents, the current state-of-the-art technology of air filtration materials for protection against highly toxic chemicals, is mainly based on the proposal of new, innovative, efficient, environmentally friendly, and economically viable textiles that provide additional protection for people in direct contact with a chemical weapon. These are effectively intelligent textiles that possess reagents or active sites capable of degrading toxic compounds (passive-to-active protection) [5][6][7][8].

For gas masks, research is much more focused on improving the properties of the adsorbent, which is most often activated carbon (AC) for protection against chemical warfare agents [9][10][11]. A significant disadvantage of these protection systems is that the filter cartridges have limited autonomy, thus reducing the action time of the personnel involved [12]. Consequently, regularly changing them to maintain optimal protection is necessary. Thus, developing effective self-cleaning filters is crucial for guaranteeing the safety of personnel intervening in emergencies, particularly CBRN situations.

This work is part of this protection context. Indeed, treating (or simulating) toxic gases by coupling adsorption and photocatalysis is of interest. The association between the two processes is based on the adsorbent allowing for temporary storage during peak exposures and photocatalyst activation improving the adsorption of the pollutant and restoring the active sites by degrading the stored contaminant into CO_2 and H_2O [13–17]. This work aimed to remove scientific obstacles to designing a compact, self-contained filtration cartridge for individual protection for intervening in and managing CBRN emergencies.

Adsorptive removal and photocatalytic oxidation are two effective technologies for efficiently removing toxic compounds. The literature has shown that most of the work on coupling the two processes focuses on developing hybrid compounds based on nano-photocatalysts and an adsorbent [18][19]. The interest in this combination is to develop efficient process, usually based on TiO_2 with excellent recycling properties for practical application in the degradation of high-concentration pollutants. Adsorbents can be based on adsorbent fibers, carbon nanotubes, graphene, AC and biochar [19][20][21][22][23].

Another way to link the two processes is to place the photocatalytic reactor in a series with the adsorbent filter. Wan-Kuen and Chang-Hee (2009) [24] tested the suitability of putting an adsorbing filter before a photocatalytic reactor. In this case, it was instead of an outlet protection mechanism. Thus, from the breakthrough, residues pass through the adsorbent filter, which would be harmful if no photocatalytic reactor were downstream. This configuration allows the filter to be operated longer without worrying about pollutants passing through. This solution was also used in a multidisciplinary project CUBAIR (2019) [25]. However, putting the photocatalytic reactor upstream of the adsorbing filter is more sensible. Many researchers, including Jain et al. (2007) [26] and Lim et al. (2011) [27] have analyzed this configuration. This configuration aims to delay the filter’s inevitable breakthrough and extend its life as much as possible. Furthermore, Mamaghani et al. (2021) [28] adopted a promising strategy to improve the efficiency of air treatment systems in which the combination of TiO_2 and ACF showed better efficiency than TiO_2 coated on nickel foam filter (NFF) and uncoated activated carbon fiber. Due to ACF's high affinity and adsorption capacity, MEK molecules were concentrated around TiO_2, which improved the reaction rate and led to higher removal efficiency. Nonetheless, the photocatalytic degradation of MEK could effectively increase the breakthrough time of the ACF. TiO_2 continuously oxidized the MEK adsorbed on the ACF's surface, leading to *in situ* regeneration.

Another advantage of coupling the two processes in a series is the possibility of regenerating the adsorbent and reusing the filter several times. Yet, after a few cycles, the amount of adsorbed pollutants decreased with each regeneration until the filter became inefficient. Considering the example of water treatment, the presence of H_2O_2 during regeneration made the adsorbent more efficient, with a higher lifetime (the number of cycles) [29].

This study applies an optimized version of photocatalytic module (optical fibers) with a regeneration process by Joule effect (in situ heating) developed for the regeneration of an AF support saturated with chemical warfare agent simulants (mustard), methyl salicylate and Diethylsulphide.

The device combining the photocatalytic process with an adsorbent was also tested for continuous treatment under realistic conditions in a climatic chamber in the presence of a dummy (FeTHeMa), with the aim of proposing a new advanced technique for respiratory protection against highly toxic chemical compounds with an active aspect.

This detailed study aims to overcome the scientific barriers to the design of a compact, self-contained filter cartridge for personal protection in CBRN emergency management and response, in line with the Sustainable Development Goals (SDGs).

The literature review did not reveal any work presenting a compact configuration coupling the photocatalytic process on luminous tissue with an adsorption process with an integrated regeneration pathway, especially considering that the coupling configuration has been developed and tested for chemical warfare agent treatment applications.

2. Material and methods

2.1. Pollutants studied

In this study, target molecules were chosen for specific reasons, converging on the effectiveness of respiratory protection. Accordingly, the first compound is cyclohexane, a reference for the effectiveness tests of type A anti-gas filtration cartridges [12][30]. The second compound was a simulated mustard gas with sulfur ($C_4H_8Cl_2S$), namely methyl salicylate ($C_8H_8O_3$), a compound in which studies of adsorption and desorption showed that it effectively mimicked the behavior of mustard gas [31][32][33][34].

Since mustard gas is a sulfur compound, validating its degradation and the system’s performance against a sulfur compound was necessary. Therefore, sulfur diethyl (C_2H_6S) was chosen for these tests [35][36][37,38].

Sigma-Aldrich provided the studied compounds in a liquid form with purities of >98%, >99%, and >98% for cyclohexane, methyl salicylate, and sulfur diethyl, respectively, which volatilized obtaining the desired gas concentrations.

2.2. Supports

2.2.1. Photocatalytic support

The photocatalytic substrate tested during this study was a new double-sided optical fiber (OF) photocatalytic media manufactured by Brochier Technologies (UVtex®) (Fig. 1a), with TiO_2 (Degussa P25) deposited equal to 26 $g.m^{-2}$. Previous publications have presented further information on these media [39][40][41]. Details on the manufacturing process of the media and the results of a characterization of the surface texture of the photocatalytic media by scanning electron microscopy (SEM-JEOL JSM 7100F) (Fig. S1 and S2) are provided in supporting information [42][43][44].

2.2.2. Adsorption supports

In this work, adsorption media provided by the DACARB was used (Fig. 1b). It was made of activated carbon felt (AF) under the reference FEU-CS-V-4 and manufactured based on viscose at high temperatures and in the presence of water vapor. This support had a specific area of 1,100 $m^2.g^{-1}$ with a pore volume of 0.8 $cm^3.g^{-1}$, 40% of which was mesoporous; a thickness of 4 mm; and a weight of 250 $g.m^{-2}$.

The supplier communicated the AF's surface functions. The main surface functions were carboxylic (0.01 $mmol.g^{-1}$), phenolic (0.17 $mmol.g^{-1}$), and basic (0.20 $mmol.g^{-1}$).

2.3. Reactors and experimental devices:

2.3.1. Reactor configuration

The reactor represented the construction of a new front-flow reactor configuration (Fig. 1c), based on the same principle of chaining photocatalytic and adsorbent media. The cross-section was 10 × 10 cm. The reactor was made of Bakelite, which gave it high mechanical resistance (hard, rigid), electrical insulation, and good temperature resistance (120 C°). The objective of this configuration was to optimize photocatalytic treatment by reducing the residence time while ensuring good degradation efficiency. This latter configuration was called PFR-LED optimized.

The PFR-LED reactor compartments were also adapted for installing adsorbent support, in which two copper rods were integrated. Thus, the regeneration step was conducted using the Joule effect. Therefore, installing copper electrodes in the reactor compartments ensured the necessity of electrical connections.

The main characteristics of the photocatalytic module configuration are presented in Table S1.

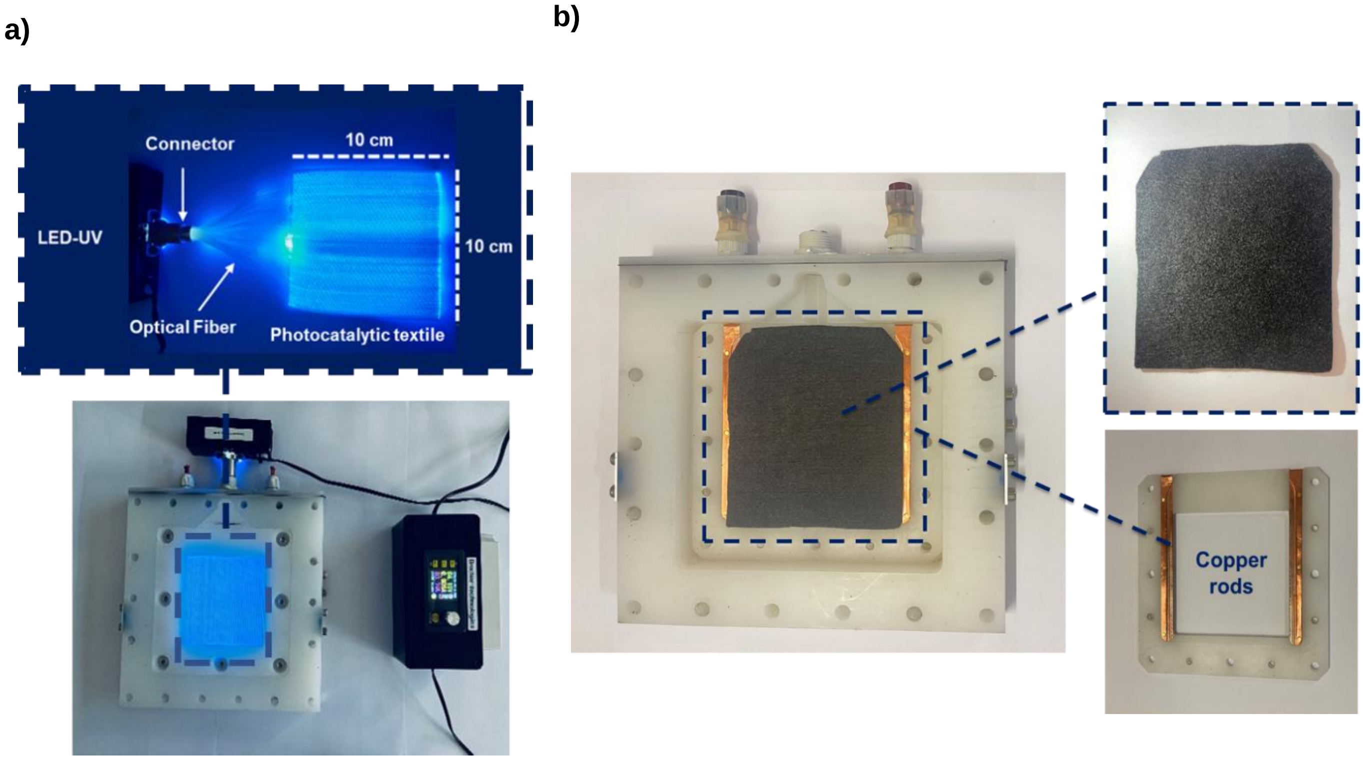

Photocatalytic support with TiO_2 coated on Optical fiber

Activated carbon felt (FEU-CS-V-4) ''AF'' support

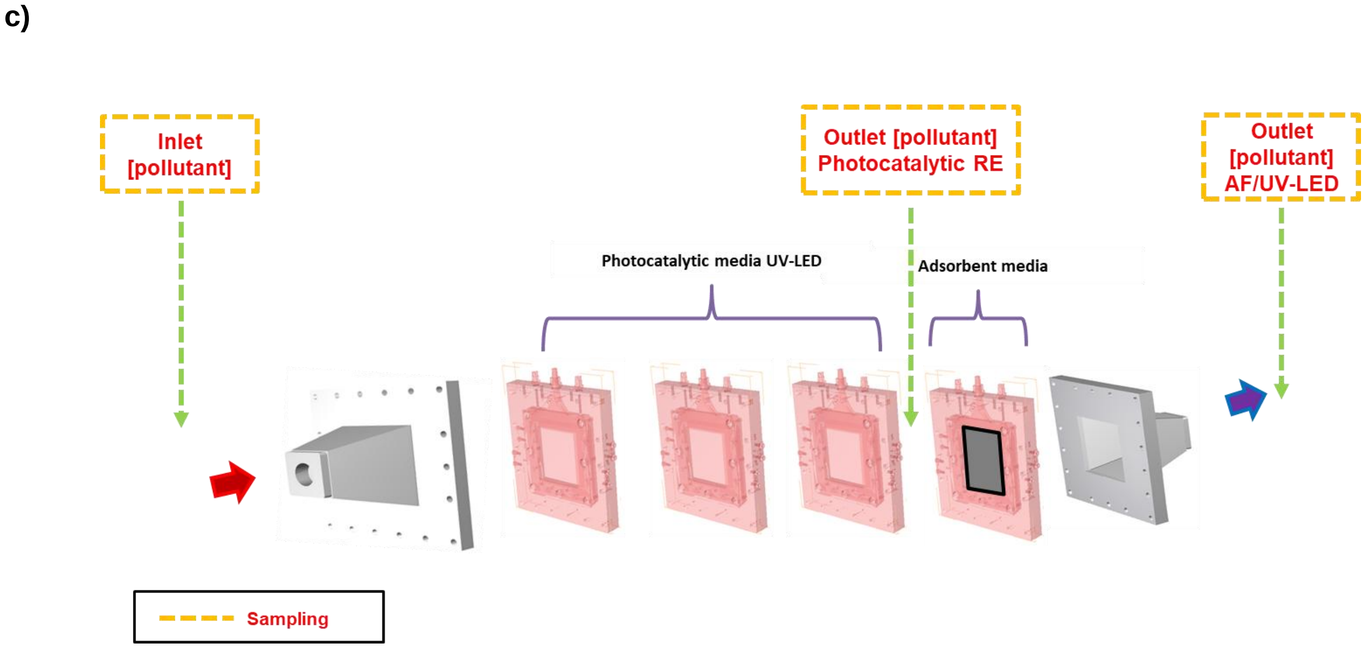

Photocatalytic front flow module based on Luminous tissue and AF filter

Figure 1: Front-flow module based on a) optical fibers photocatalytic media (PFR-LED) coupled to b) AF supports

179

2.3.2. Experimental setup

The system consisted of two configurations. One was for a continuous treatment in which dry air returning from the network was the carrier gas. A mass flow meter controlled its flow (Bronkhorst In-Flow). A bubbler containing water was installed in the circuit to humidify the air. The pollutant was continuously injected in liquid form by a syringe and pump assembly. A heating ribbon was placed in the injection zone to facilitate the pollutant's volatilization. A static mixer allowed for the upstream homogenization of the reactor's effluent. Two septa downstream and upstream of the photoreactor allowed for sampling outlet and inlet gas with a syringe. The second configuration was a closed-loop treatment in which a recirculation flow (about 1 $m^3.h^{-1}$) was dedicated to studying adsorbent regeneration.

The desorption device used a Joule effect heating system (*in situ* heating). A 600 W DC generator XG-60-14 (Amatek®) with voltage and working current ranges of 0–60 V and 0–10 A, respectively, was used. This system provided an electrical circuit with a current of 5 A and a voltage of 35 V for thermal conduction heating of the adsorbent media. To maintain the desorption temperature at a temperature level of 70 ± 2C° throughout the experiment, a thermostat was set up and equipped with a chromium-nickel alloy probe, with a linear response over the range of 0–1,000 K installed on the support's surface. A temperature sensor was also installed at the reactor entrance connected to an Arduino system, allowing one to follow the temperature evolution by direct data acquisition on a PC. This system permitted the maintenance of the necessary temperature for desorption throughout the experiment.

Figure 2 shows the experimental procedure.

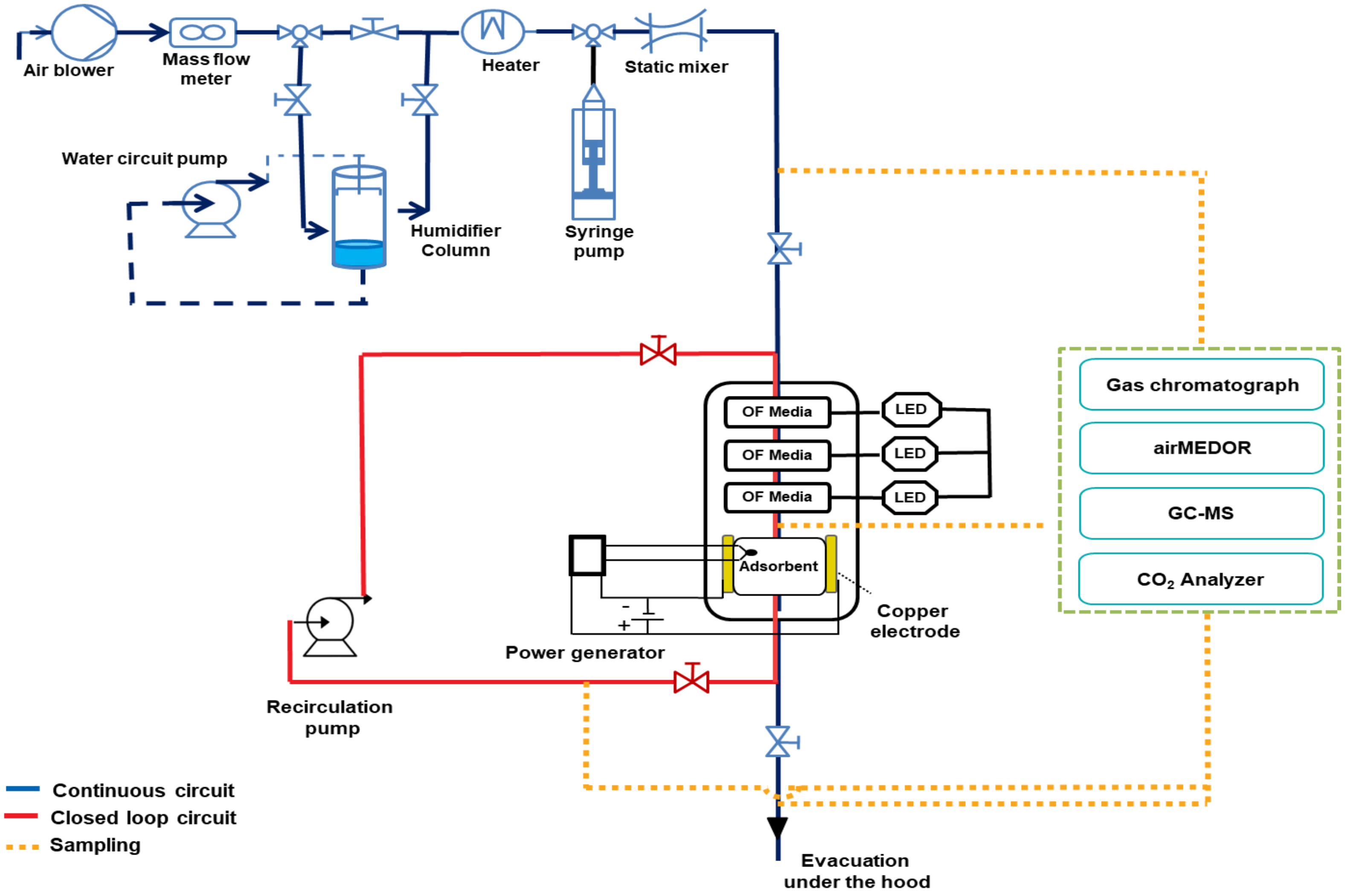

Figure 2: Diagram of the installation of the coupling configuration of the adsorbent with photocatalytic process with different desorption methods.

2.4. Climatic chamber for full-scale tests

The experiments were conducted in the climatic chamber QUALIDIF of the LGCGM Laboratory (Fig. 3a) with the following dimensions: L× W × H = 3.50m × 3.50 m × 2.50 m. It was coupled to an air diffusion circuit, including an air handling unit (AHU).

The six inside faces were thermally controlled using a hydraulic circuit composed of PER pipes inserted into the walls and connected to a heat pump for simultaneous heating and cooling. The ambient temperature in the chamber was controlled with a hydraulic circuit. The AHU generated by a ceiling air jet was equipped with a fan, a heater, a chiller, and a CELLKRAFT stream generator E-6000 with an external humidity sensor for accuracy ±(1.5 + 0.015 x reading), followed by a plenum box. The air diffusion terminal unit was installed at the extremity of the plenum box. The inlet flow rate and air temperature were controlled with sensors placed between the handling unit and the plenum box and again measured at the jet exit using an ACIN balometer (Flowfinder mk2). The accuracy in the flow rate measurement was ±3% of the reading. The air returned to the AHU via an outlet at the bottom of a wall. This return air was not mixed with fresh air from the outdoors; the AHU recirculated the air already present in the chamber via airtight pipes.

The chamber was equipped with air temperature sensors (PT1000_1/3 DIN – accuracy of ±0.1°C) and omnidirectional anemometers (TSI 8475, accuracy of ±3% of the reading) to determine the RH percentage. Cameras were present in the chamber to view the interior from the outside of the chamber.

The climatic chamber was also equipped with a humanlike thermal manikin (named FeTHeMa, based on “female thermal manikin”; see Fig. 3b), mimicking the human body due to 79 thermoregulated zones. This manikin was developed according to the standard ISO 14505–2:2006, noted in P. Danca's [45] thesis on local thermal comfort measurement. A supplementary breathing system was integrated into the manikin to study pollutant concentrations in the inhaled air when an ambient exposition risk exists. In the present study, the twin tubes connecting the manikin's nostrils to the outside were attached to a pump. In the first step, the air samples in this (respiratory) circuit were analyzed in the presence of cyclohexane C_6H_{12} [12] (a reference for testing the effectiveness of anti-gas filter cartridges) in the chamber, which represented the reference case of exposure. In the second step, the (respiratory) circuit was connected to the filtration module (PFR-LED Optimized coupled to AF support). The analysis of the filtered air at the outlet of the cartridge enabled the testing of the effectiveness of the cartridge to protect anyone exposed to the chemical agent. An air sampling system was installed in the chamber (Fig. 4) to determine the various sampling points inside the room. It also monitored the concentration of the pollutant at the inlet and outlet of the purification reactor from outside the climate chamber.

(a)

(b)

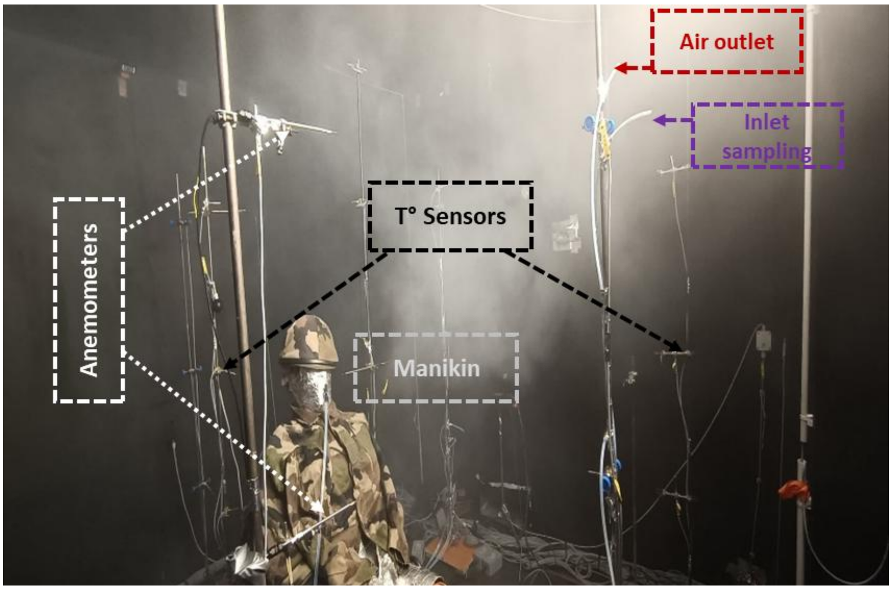

Figure 3: a) Climatic chamber QUALIDIF and FeTHeMa thermal Manikin b) in a contaminated area.

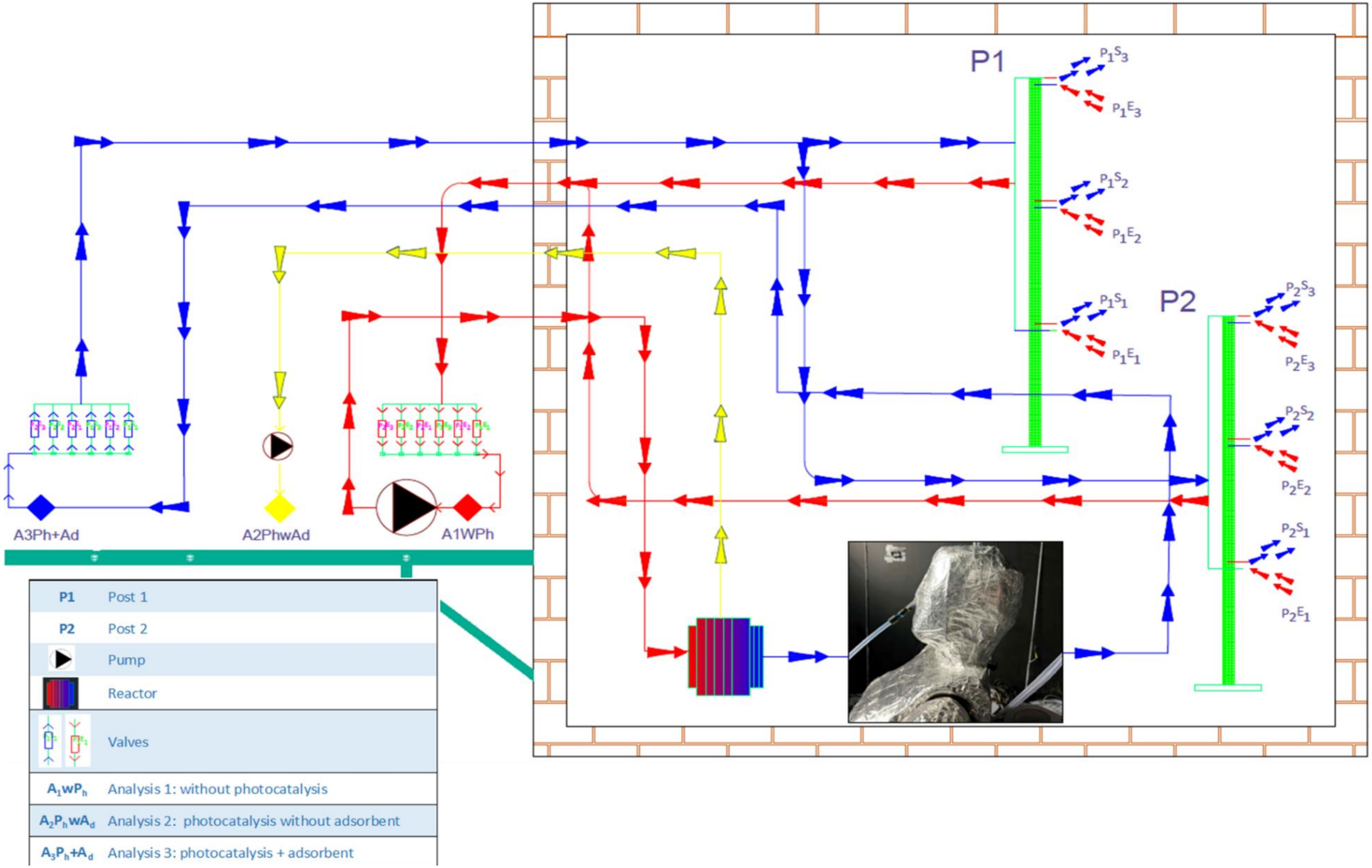

P1	Post 1
P2	Post 2
▶	Pump
	Reactor
	Valves
A_1wP_h	Analysis 1: without photocatalysis
$A_2P_hwA_d$	Analysis 2: photocatalysis without adsorbent
$A_3P_h+A_d$	Analysis 3: photocatalysis + adsorbent

Figure 4: Experimental principle diagrams of purification tests in realistic situations.

2.5. Analytic tools

Different main factors were considered for evaluating the performance of the different photocatalytic configurations and coupling modules, such as the adsorption capacity of the adsorbent media in the dynamic tests. The adsorption capacity was calculated using Eq.1:

$$q_e = \frac{M_e}{M} \quad \text{where, } M_e = Q \int_0^\infty (C_e - C)\, dt \qquad (1)$$

q_e is the adsorption capacity ($g_{pollutant}$ / $g_{adsorbent}$); C_o and C are the initial and instantaneous concentrations at a given time, respectively; and Q and t are the adsorbate flow rate ($L.min^{-1}$) and time (min), respectively.

The breakthrough adsorption behavior was predicted using Clark's dynamic adsorption model [46]. This model was based on the concepts of mass transfer, which consider the dynamic phenomenon and isothermal Freundlich equation representing equilibrium. They were also based on the assumption that fluid flow is of a piston type. The model's equation is expressed as follows:

$$\frac{C_s}{C_0} = [\frac{1}{1 - A\, e^{-rt}}]^{1/(n-1)} \qquad (2)$$

The breakthrough time is expressed using Eq. 3:

$$tp = \frac{lnA - ln\, (\frac{C_0{}^{n-1}}{Cp^{\,n-1}} - 1)}{r} \qquad (3)$$

The material balance and the energy balance of electrical power consumed during the regeneration process were the basis for a better evaluation of regeneration performance, the average specific elimination rate, and the desorption rate:

$$Average\ elimination\ rate = Mass\ eliminated\ / Degradation\ time\ /\ Mass\ of\ TiO_2 \quad (4)$$

$$Desorption\ rate\ =\ desorbed\ mass\ of\ pollutant\ /\ Desorption\ time \quad (5)$$

$$E_{consumed} = E_{regneration} = E_{desorption} + E_{Photocatalyse} \quad (6)$$

2.6. Analytical Instruments

The different analytical methods used in this work are detailed in the information material. The studied gases were analyzed using two gas-phase chromatographs coupled to an FID detector. One had an FFAP column for analyzing cyclohexane, and the other had an HP5 column for analyzing methyl salicylate. Sulfur diethyl was analyzed using airMEDOR. Detailed information about the analysis setup was presented in previous work [47].

3. Results and discussions

3.1. Study of adsorbent regeneration by a photocatalytic module

The adsorption performance of the used support was developed in a batch study to highlight its effectiveness in retaining the selected pollutants [48][49]. Table S2 summarized the results of the adsorption parameters. The order of magnitude of the obtained adsorption capacities was consistent with those in the literature [12], Freundlich and Langmuir models provided a good correlation of the experimental results.

3.1.1 Adsorption and desorption cycle studies of AF media with the PFR-LED Optimized module during in situ regeneration

This study aimed to evaluate the evolution of the adsorption capacities of AF media during adsorption–desorption cycles in the same sample. For this purpose, different regeneration cycles were conducted on the adsorbent medium (AF) by *in situ* desorption with an optimized PFR-LED photocatalytic module (Fig. 5). The concentration of MS injected to obtain adsorption equilibrium, the operating conditions, and the electrical power applied for desorption were kept identical for each cycle. Monitoring of the absolute humidity during the regeneration process was also implemented to better evaluate the photocatalytic degradation of the pollutant during the regeneration process. Notably, the adopted saturation rate corresponded with the respiratory rate for light physical activities, and the saturation rate corresponded with the respiratory flow rate for light work in accordance with the ISO standard ISO/DIS 8996 [50].

The material balance (Fig. 6a) was based on an analysis of the amount adsorbed during different adsorption cycles. The results of the balance showed a decrease in the adsorption capacity of the AF media after each regeneration cycle (8.01 mmol in cycle 1 and 7.81 mmol in cycle 2) compared to the amount adsorbed at the beginning (8.44 mmol). The regeneration rate (Fig. 6b) confirmed this finding, in which a loss was observed after each regeneration cycle. A decrease in the working time of the filter was also recorded after each regeneration cycle (a decrease of 15.49% and 31.59% after the first and second regeneration cycles, respectively) (Fig. 6c). This decrease in the performance of the AF media may have been due to the incomplete regeneration of the media. This incomplete regeneration could be because of the limitation of the photocatalytic reaction on the sites as a result of competition with water molecules, as many researchers have noted [51][52][53][54][55]. Figure 6 shows an increase in absolute humidity during the regeneration of the AF generated by the photocatalytic process until reaching saturation level.

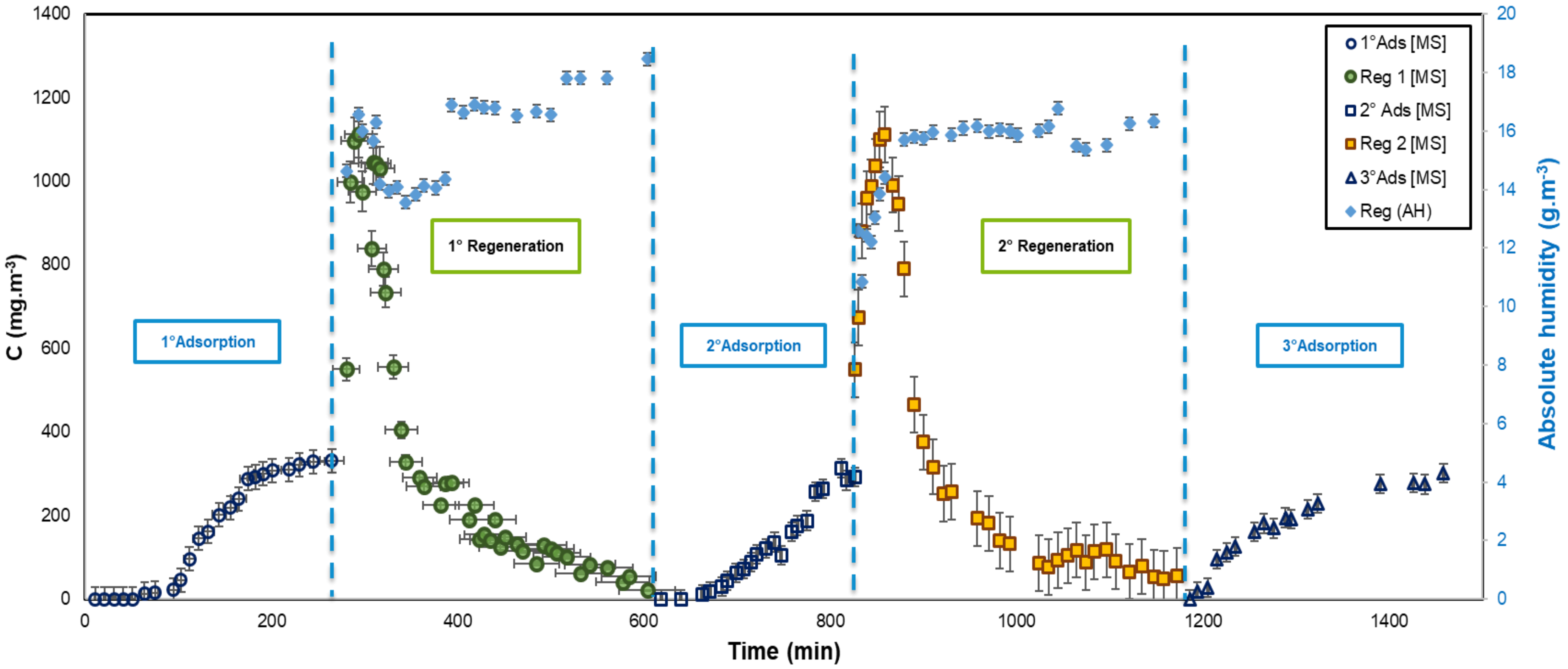

Figure 5: Adsorption and regeneration cycles of AF with optimized PFR-LED photocatalytic configuration, with absolute humidity monitoring: PFR-LED (Optimized) (m_{TiO2} = 0,78 g, I= 7,8 W.m^{-2}, m_{AF} = 2,5 g). Methyl Salicylate : C = 300 mg.m^{-3} / Q = 18 L.min^{-1} / HR = 40 ±2 %, T= 20 ±2 C°, $T_{\textit{in situ}}$ = 70 C° (35 V- 5 A), $Q_{recyrculation}$ = 1 m^{3}.h^{-1}.

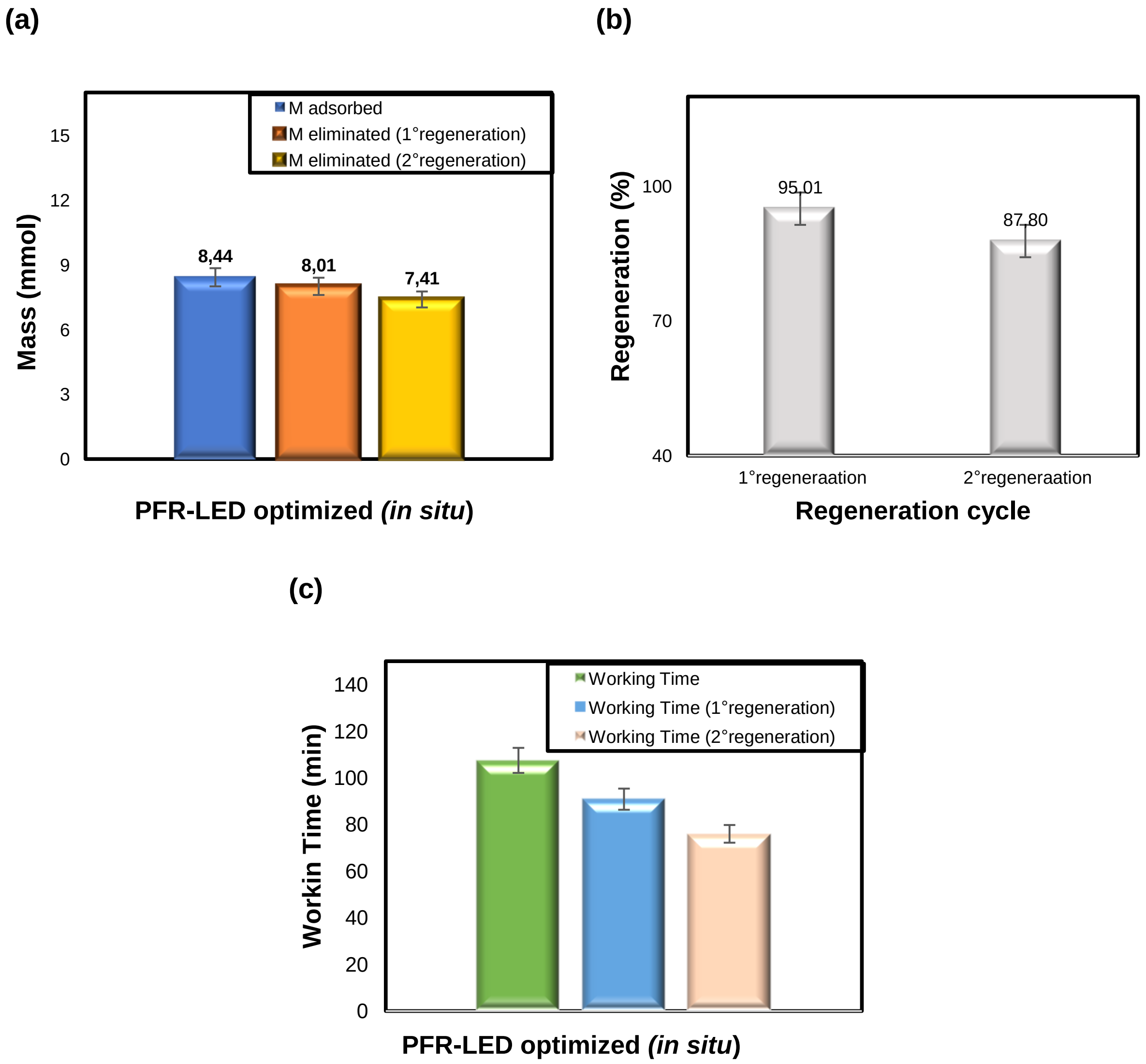

Figure 6: (a) Mass balance and (b) Regeneration rate and c) Working Time: PFR-LED (Optimized) (m_{TiO2} = 0,78 g, I= 7,8 W.m^{-2}, m_{AF} = 2,5 g). Methyl Salicylate : C = 300 mg.m^{-3} / Q = 18 L.min^{-1} / HR = 40 ±2 %, T= 20 ±2 C°, $T_{in\ situ}$ = 70 C° (35 V- 5 A), $Q_{recyrculation}$ = 1 m^{3}.h^{-1}.

Furthermore, byproducts formed during the regeneration process by photocatalytic degradation, such as benzoic acid, were not desorbed [55]. There was also the phenomenon of the depletion of the adsorbent material, which the literature has noted [56][57]. Figure 7 shows the byproducts of the photocatalytic degradation of methyl salicylate analyzed by GC-MS, where the sample was collected by concentration on CarbotrapTM (CA). From 0.1 to 1 L of gas was injected using a thermal desorber (Dynatherm Analytical Instruments, model 890) with a desorption temperature of 170 °C.

The average desorption rate, the average removal rate, and the energy consumed through the process are presented in Figure S3.

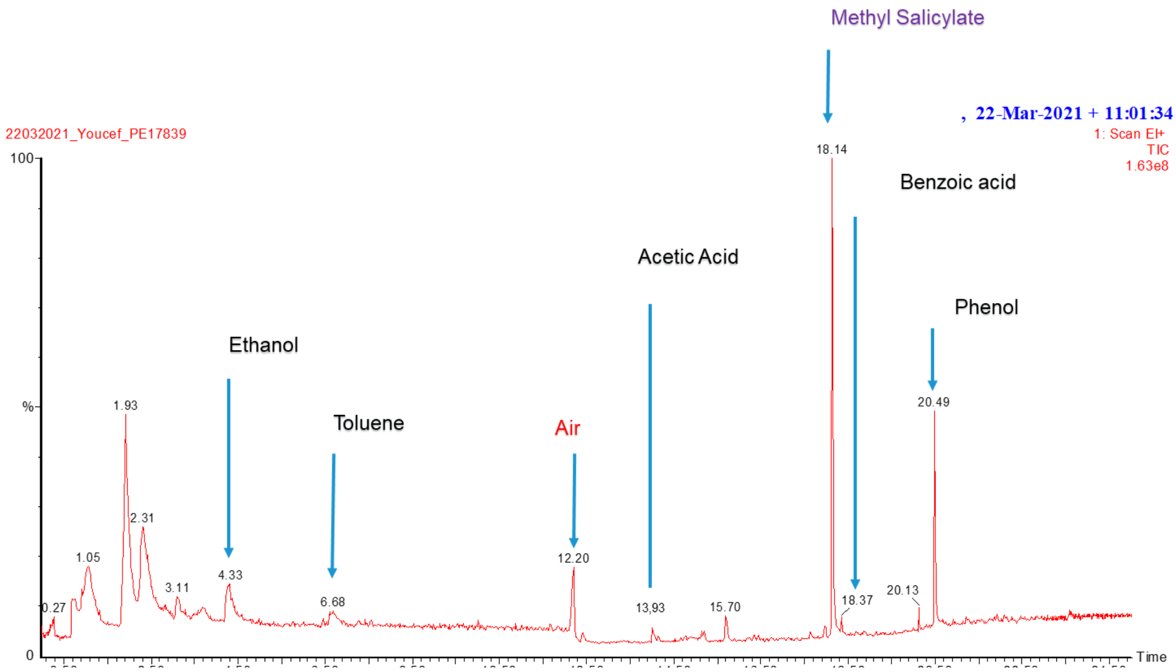

Figure 7: Photocatalytic degradation of the byproducts of methyl salicylate

3.1.2 Performance study of the AF/PFR-LED Optimized process toward the sulfur compound (Yprite “sulfur mustard”)

Since mustard is a sulfur compound, it was necessary to determine how the coupling system behaved toward it. A closed-loop treatment to regenerate the DES-saturated AF medium was studied. Of course, a final adsorption cycle must occur to reach equilibrium.

During this experiment, the formation of the degradation byproducts and the absolute humidity were monitored. The results are presented in Figure 8.

(a)

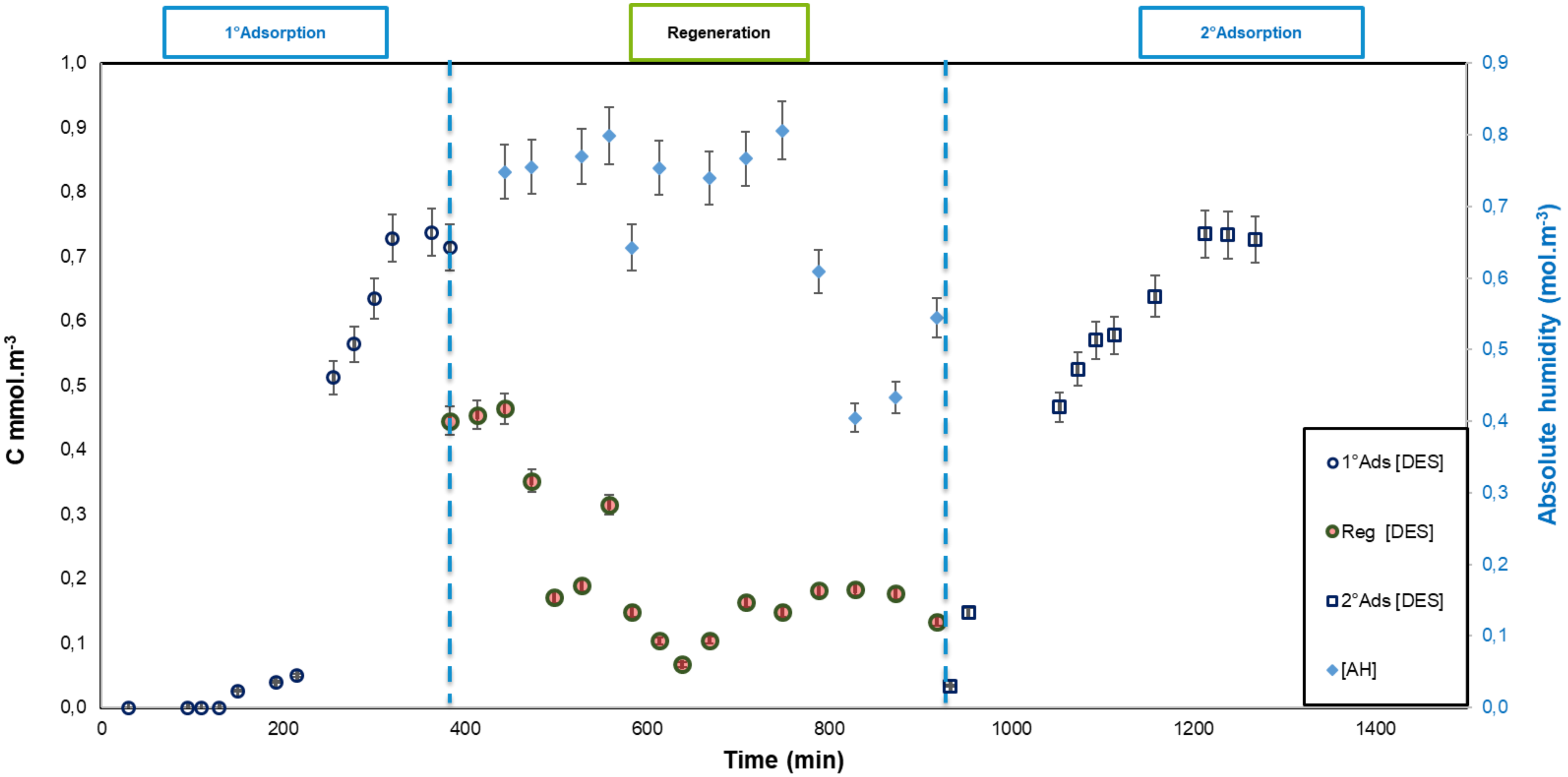
1°Adsorption
Regeneration
2°Adsorption
C mmol.m-3
Absolute humidity (mol.m-3)
Time (min)
1,0
0,9
0,8
0,7
0,6
0,5
0,4
0,3
0,2
0,1
0,0
0
200
400
600
800
1000
1200
1400
0,9
0,8
0,7
0,6
0,5
0,4
0,3
0,2
0,1
0,0
1°Ads [DES]
Reg [DES]
2°Ads [DES]
[AH]

(b)

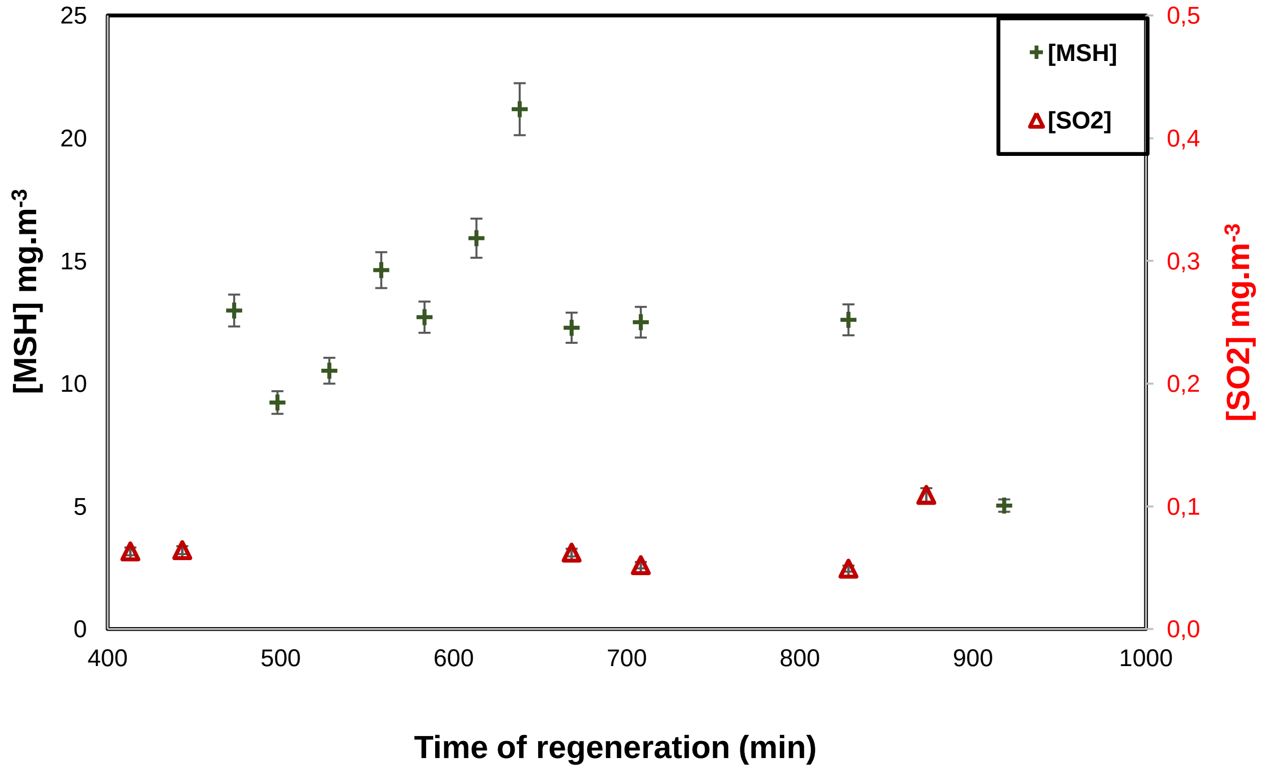

Figure 8: a a) Adsorption under UV and the regeneration cycle of AF with optimized PFR-LED photocatalytic configuration with absolute humidity monitoring: PFR-LED (optimized) and b) the evolution of the byproducts during the regeneration cycle. (m_{TiO2} = 0.78 g, I = 7, 8 $W.m^{-2}$, m_{AF} = 2.5 g). Sulfur diethyl: C = 0.9 $mmol.m^{-3}$/Q = $L.min^{-1}$/HR = 40 ± 2%, T = 20 ±2°C, $T_{in\ situ}$ = 70°C (35 V- 5 A), $Q_{recyrculation}$ = 1 $m^3.h^{-1}$.

The analysis of the results also indicated a regeneration rate of AF support of 76.92%. This incomplete regeneration could be due to poor desorption of DES [56] and the byproducts' degradation in which the phenomenon of competition occurred, as reported in the literature [40][57], namely the SO_2, which is known for its tendency to poison the catalyst (TiO_2) [58][59]. Moreover, an abundance of MSH was initially seen in the formation of intermediates due to the desorption of the target compound. The MSH formed was then degraded to ultimately form SO_2. This mechanism aligned with the literature [5][60] for the degradation of DES, according to the mechanism shown in Figure S4.

3.2. Continuous coupling study

3.2.1 Continuous coupling for the Methyl salicylate treatment

As previously mentioned, one configuration of adsorption and photocatalysis coupling was the installation of the photocatalytic module upstream of the fixed adsorption bed. The few authors who have studied continuous coupling to increase the running time of the adsorption filter favor this solution [26][27] .

In this study, a photocatalytic module was placed upstream of an AF adsorption filter to perform an air purification test with the mustard gas simulant MS. A comparative study between classical adsorption with an AF filter alone and another one based on the AF/UV-LED coupling was also presented. In this study, sampling was performed at the inlet of the system, after the photocatalytic module in order to estimate its performance and a last one at the outlet of the coupling system (after the module and the adsorbent filter). The sampling system is shown in an explanatory diagram in Figure 9a:

(a)

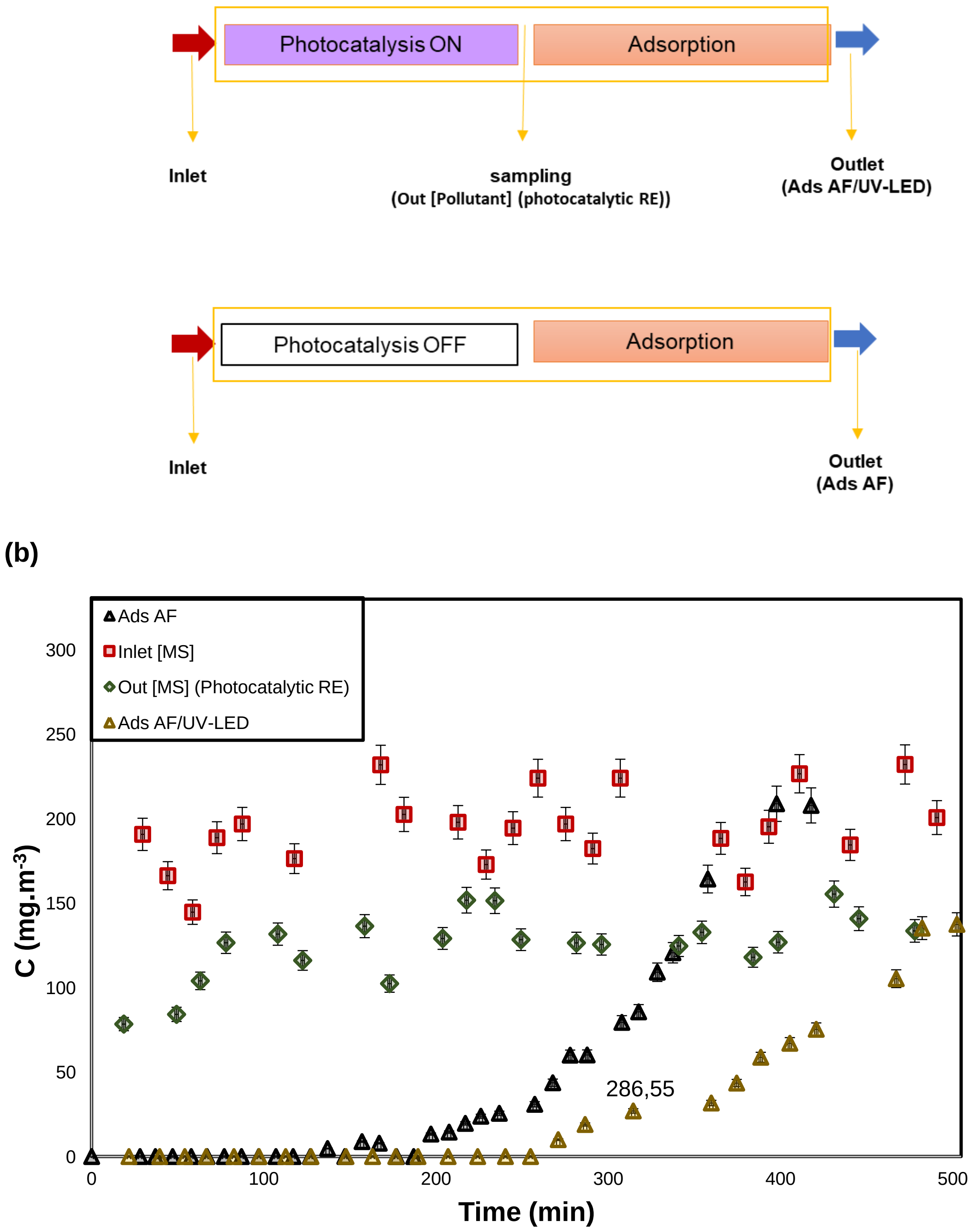

Figure 9: a) Sampling schematic and b) the result of continuous treatment of methyl salicylate with AF support alone and with front-flow photocatalytic optimized PFR-LED coupled with AF support: (m_{TiO2} = 0.78 g, I = 7.8 $W.m^{-2}$, m_{AF} = 2.5 g). Methyl calicylate: C = 200 $mg.m^{-3}$/Q = 18 $L.min^{-1}$/HR = 40 ± 2%, T = 20 ± 2°C.

Figure 9b shows the concentration of methyl salicylate during adsorption with activated carbon felt alone and with a combination of the optimized PFR-LED photocatalytic module and the activated carbon felt. The MS concentration at the outlet of the photocatalytic section was also measured to evaluate the photocatalytic process's performance.

The results indicated that using a photocatalytic module upstream allowed for a significant degradation of the pollutant, estimated at 36% of removal efficiency over the entire treatment time (RE_{moyen}) with a CO_2 selectivity of 15%. This led to the adsorbent support receiving decreased concentration [27][28]. This increased the filter operating time by about 20%, resulting in a corresponding change in breakthrough time (5 h versus 4 h for AF alone).

The equilibrium adsorption capacity was estimated at 0.61 $g_{MS}.g_{AF}^{-1}$ for adsorption alone and 0.48 $g_{MS}.g_{AF}^{-1}$ for adsorption from the coupling. The equilibrium adsorption capacity decreased proportionally to the input concentration, and the breakthrough time increased when the latter decreased. This finding could be explained by the fact that the higher the input concentration of the target gas, the greater the number of molecules that can be adsorbed. Similarly, the breakthrough and saturation times were shortened [61][62][63].

3.2.2 Simulating exposure to chemical toxins in a real environment

This study focused on human respiratory safety in toxic environments. Accordingly, an optimized PFR-LED photocatalytic module and AF were tested to ensure the respiratory protection of a FeTHeMa thermal manikin. The challenge was to validate a solution that would save time on filter life, namely continuous process coupling while maintaining a comfortable thermal and ventilation environment. The FeTheMa thermal manikin is used as an inhaled air quality assessment tool and as a thermal comfort sensor.

Before proceeding with the filtration coupling tests, it was essential to determine the system's tightness and the contamination's homogeneity inside the chamber. Therefore, different tests were conducted, namely a smoke test (Fig. S5) to determine potential pollution and dead spots and a homogeneity test of the concentration inside the environmental chamber (blank test). The conditions of the environmental chamber and the thermal comfort of the manikin were also monitored during these tests. The details and results of this section are summarized in the supporting information. When the closed system allowed for a homogeneous concentration over the entire chamber volume (Fig. S6), the system did not significantly impact climatic conditions (Fig. S7). Moreover, the thermal comfort on the different parts of the manikin's body was homogeneous (Fig. S8).

The tests were performed with an approximate respiratory flow rate for intense work, according to the previously mentioned ISO/DIS 8996 standards.

(a)

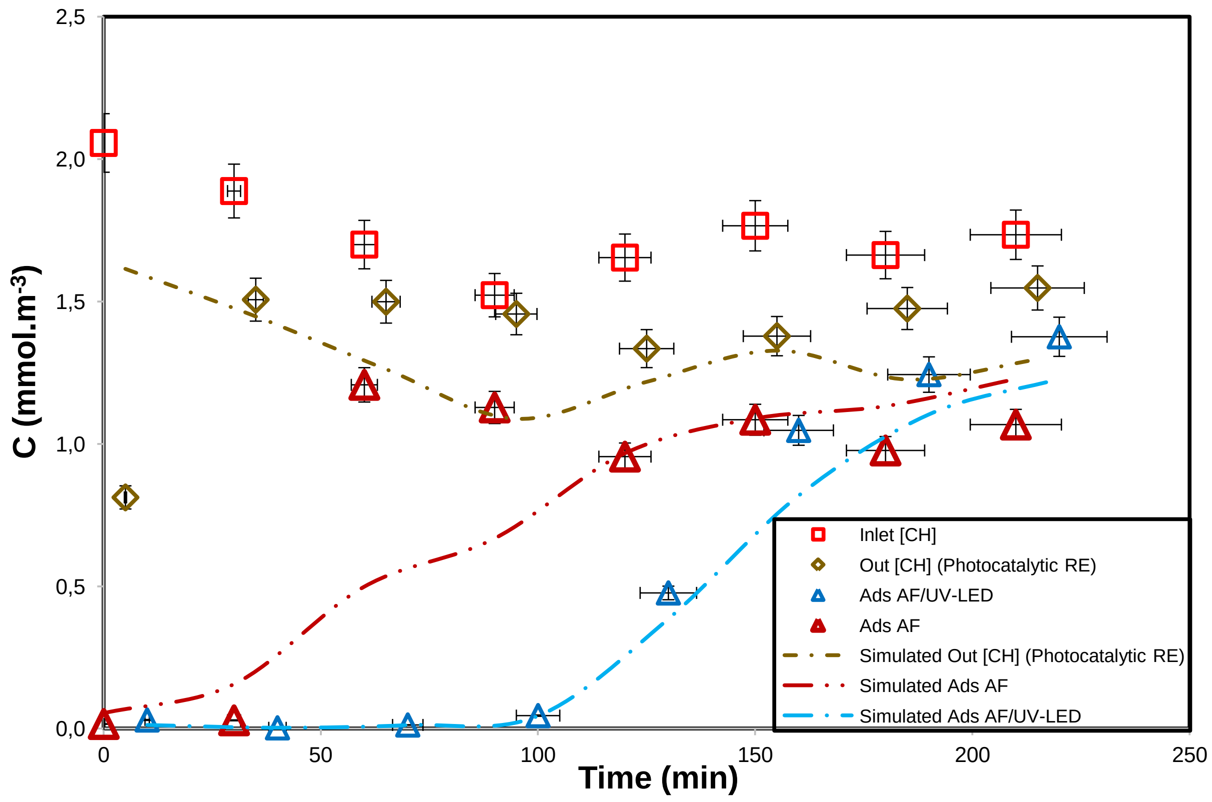
C (mmol.m^{-3})
2,5
2,0
1,5
1,0
0,5
0,0
0
50
100
150
200
250
Time (min)
Inlet [CH]
Out [CH] (Photocatalytic RE)
Ads AF/UV-LED
Ads AF
Simulated Out [CH] (Photocatalytic RE)
Simulated Ads AF
Simulated Ads AF/UV-LED

(b)

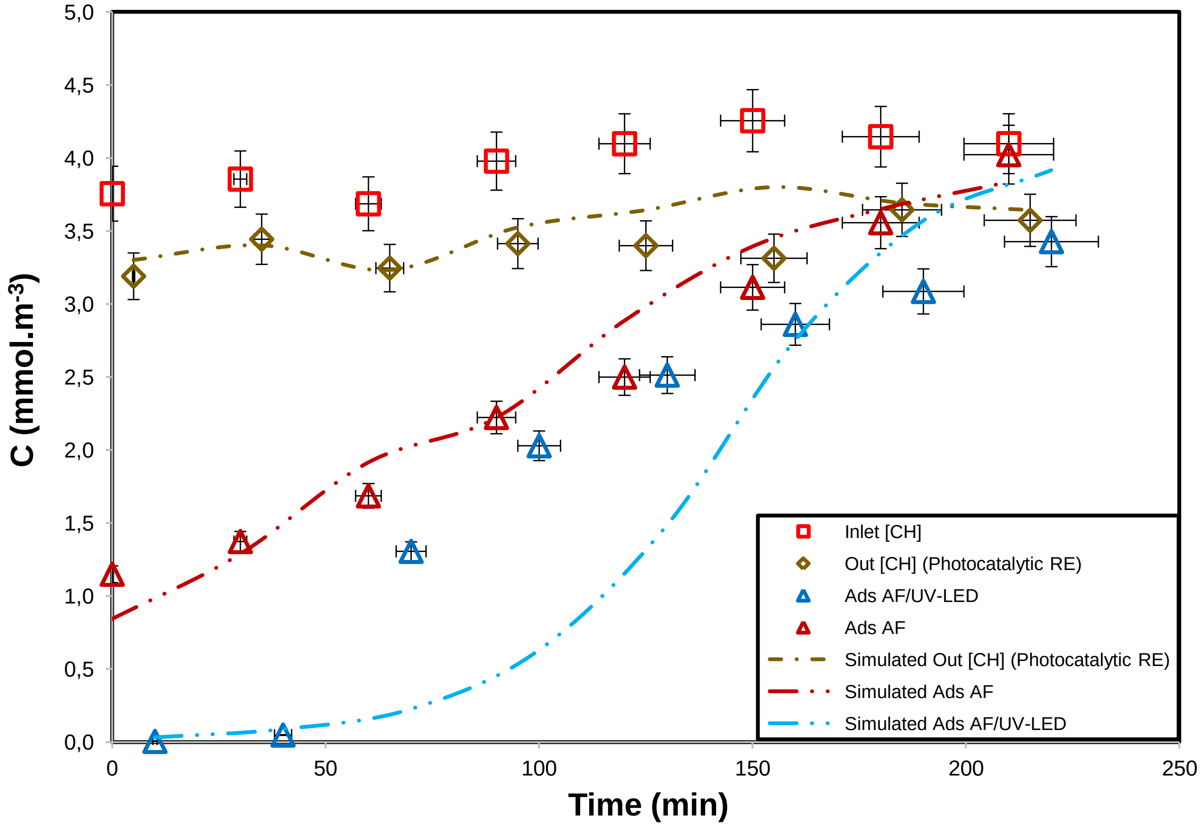
C (mmol.m^{-3})
5,0
4,5
4,0
3,5
3,0
2,5
2,0
1,5
1,0
0,5
0,0
0
50
100
150
200
250
Time (min)
Inlet [CH]
Out [CH] (Photocatalytic RE)
Ads AF/UV-LED
Ads AF
Simulated Out [CH] (Photocatalytic RE)
Simulated Ads AF
Simulated Ads AF/UV-LED

Figure 10: Continuous treatment of cyclohexane with AF support alone and with front-flow photocatalytic optimized PFR-LED coupled with AF support at different concentrations of the pollutant a) [CH] = 150 and b) 300 mg.m^{-3} (m_{TiO2} = 0.78 g, I = 7.8 W.m^{-2}, m_{AF} = 2.5 g)/Q = 25 L.min^{-1}/HR = 44 ± 2%, T = 22 ± 2°C.

Figures 10a and 10b show the air quality that FeTHeMa breathed. They compare the quality of the air filtered with adsorbent AF alone and the air filtered with adsorption coupled with the upstream optimized PFR-LED photocatalytic module. The room had different contamination rates, but the same climatic conditions were maintained for the different tests. The concentration of the pollutant in the air to be breathed was measured at different points of the system, namely, the concentration at the inlet, after the photocatalytic module, and the concentration at the outlet of the filtration system, the latter representing the actual concentration that the manikin received.

The results showed that the upstream implementation of photocatalysis allowed for relieving the AF adsorbent by lowering the concentration of the pollutant received by the latter, extending its duration of use by allowing the dummy to breathe clean air for 60 and 30 min (Fig. 10a and 10b, respectively, referencing breakthrough time) more than during air filtration with AF alone.

The results also showed similar behavior to what has been reported in the literature on the effect of concentration. Such behavior was found in photocatalysis and its limitation at high concentrations due to the unavailability of active sites [64–66], It was also found in adsorption, in which the higher the input concentration of the target gas was, the greater the number of molecules that could be adsorbed, consequently decreasing the breakthrough time [67][68][69][63].

The results were simulated using a model proposed in the authors' previous work [70] to describe the experimentally observed degradation. Details of the model are provided in the reference paper. This model considered the reaction on the photocatalytic surface and the mass transfer step Eq. S7 in the supporting information. The kinetic constants (k and K) were obtained during laboratory tests at different concentrations for different flow rates for the photocatalytic degradation of cyclohexane with the optimized PFR-LED module, whose degradation efficiency results were presented in the authors' previous work [41], The results of the modeling are shown in Figure S9, in which a good fit of the experimental laboratory results with the simulated results was noted.

This model also allowed for a good description of the experimental results under real environmental conditions (Fig. 10a and 10b), in which the concentration resulting from the simulated photocatalytic module (Simulated Out [CH] (photocatalytic RE)) was in agreement with the experimental concentration (Out [CH] (photocatalytic RE)) [66][71][72]. The Clark model also simulated the breakthrough curves to evaluate adsorption with and without the photocatalytic module. The model correlates well with the experimental results.

Notably, the pressure drop in this purification system based on the coupling of the optimized PFR-LED photocatalytic module and the AF filter was estimated at 9 Pa. This finding suggests the possibility of adding photocatalytic or adsorbent compartments for better treatment efficiency, as indicated in previous work [41], while remaining within the range of the pressure drop tolerated for anti-gas filtration means (i.e., protective masks) [73].

The analysis of the thermic comfort of the different body parts of the manikin showed a normal state and stability throughout the experiment (Fig. S8).

4. Conclusions

This study considered using photocatalysis and adsorption coupling to treat chemical warfare agents, in which mustard gas simulants Methyl Salicylate and Diethyl Sulphur were tested.

To regenerate an adsorbent filter, the photocatalytic module was improved by implementing Joule desorption (*in situ*), thus increasing the regeneration of the adsorbent. However, and as already expected, the results showed a decrease in the adsorption performance of the support after each regeneration cycle. The optimized coupling system was also tested to cope with the sulfur compound, and the results were encouraging, counting the competition phenomenon with the by-products.

This new optimized coupling configuration with an upstream photocatalytic module was proven effective for continuously treating chemicals in the laboratory and under realistic conditions, relieving the pressure on the adsorbent filter and increasing its working time, shifting the breakthrough time by 30 min in extreme conditions.

Finally, this exhaustive investigation overcame scientific obstacles to the design of a compact, self-contained filter cartridge for personal protection in emergency response and CBRN management. This new optimized version of the adsorption and photocatalysis coupling could also have significant potential for onboard gas filtration equipment’s.

References

[1] C. Weapons, Chemical weapons convention, Chem. Eng. News. 79 (2001) 23. https://doi.org/10.1515/ci.2003.25.4.9.

[2] P. Brasser, M. Sobera, Modelling the comfort and protection qualities of chemical, biological, radiological and nuclear (CBRN) protective clothing, Woodhead Publishing Limited, 2012. https://doi.org/10.1533/9780857095572.2.238.

[3] R.B. Ormond, R.L. Barker, Chemical, biological, radiological and nuclear (CBRN) protective clothing, Woodhead Publishing Limited, 2014. https://doi.org/10.1533/9781782420408.1.112.

[4] U. Turaga, R.J. Kendall, V. Singh, M. Lalagiri, S.S. Ramkumar, Advances in materials for chemical, biological, radiological and nuclear (CBRN) protective clothing, Woodhead Publishing Limited, 2012. https://doi.org/10.1533/9780857095572.2.260.

[5] P. Barrois, Auto-Décontaminants Vis-À-Vis D'Agents Chimiques D ' Adsorption / Filtration D ' Adsorption / Filtration, (2018). HAL Id: tel-01943784 https://tel.archives-ouvertes.fr/tel-01943784.

[6] L.pez-Maya,Textile Metal Organic-Framework Composites as Self-Detoxifying Filters for. Chem. Int. Ed. 2015, 54,6790 –6794 15213773. https://doi.org/10.1002/anie.201502094.

[7] A.X. Lu, M. McEntee, M.A. Browe, M.G. Hall, J.B. Decoste, G.W. Peterson, MOFabric: Electrospun Nanofiber Mats from PVDF/UiO-66-NH2 for Chemical Protection and Decontamination, ACS Appl. Mater. Interfaces. 9 (2017) 13632–13636. https://doi.org/10.1021/acsami.7b01621.

[8] A.O. Mateescu, G. Mateescu, I. Burducea, P. Mereuta, L. Chirila, A. Popescu, M. Stroe, A. Nila, M. Baibarac, Textile Materials Treatment With Mixture of TiO2:N and SiO2 Nanoparticles for Improvement of Their Self-Cleaning Properties, J. Nat. Fibers. 19 (2022) 2443–2456. https://doi.org/10.1080/15440478.2020.1818349.

[9] J. V. Romero, J.W.H. Smith, B.M. Sullivan, L. MacDonald, L.M. Croll, J.R. Dahn, Evaluation of the SO2 and NH3 gas adsorption properties of CuO/ZnO/Mn3O4 and CuO/ZnO/NiO ternary impregnated activated carbon using combinatorial materials science methods, ACS Comb. Sci. 15 (2013) 101–110. https://doi.org/10.1021/co3001132.

[10] E. Altintig, S. Kirkil, Preparation and properties of Ag-coated activated carbon nanocomposites produced from wild chestnut shell by ZnCl2 activation, J. Taiwan Inst. Chem. Eng. 63 (2016) 180–188. https://doi.org/10.1016/j.jtice.2016.02.032.

[11] S.S. Kiani, A. Farooq, M. Ahmad, N. Irfan, M. Nawaz, M.A. Irshad, Impregnation on activated carbon for removal of chemical warfare agents (CWAs) and radioactive content, Environ. Sci. Pollut. Res. 28 (2021) 60477–60494. https://doi.org/10.1007/s11356-021-15973-1.

[12] F. Vuong, R. Chauveau, G. Grevillot, S. Marsteau, E. Silvente, C. Vallieres, Predicting the lifetime of organic vapor cartridges exposed to volatile organic compound mixtures using a partial differential equations model, J. Occup. Environ. Hyg. 13 (2016) 675–689. https://doi.org/10.1080/15459624.2016.1166368.

[13] B. Bakbolat, C. Daulbayev, F. Sultanov, R. Beissenov, A. Umirzakov, A. Mereke, A. Bekbaev, I. Chuprakov, Recent developments of TiO2-based photocatalysis in the hydrogen evolution and photodegradation: A review, Nanomaterials. 10 (2020) 1–16. https://doi.org/10.3390/nano10091790.

[14] V.K.H. Bui, T.N. Nguyen, V. Van Tran, J. Hur, I.T. Kim, D. Park, Y.C. Lee, Photocatalytic materials for indoor air purification systems: An updated mini-review, Environ. Technol. Innov. 22 (2021) 101471. https://doi.org/10.1016/j.eti.2021.101471.

[15] J. Oliveira De Brito Lira, H.G. Riella, N. Padoin, C. Soares, An Overview of Photoreactors and Computational Modeling for the Intensification of Photocatalytic Processes in the Gas-Phase: State-of-Art, J. Environ. Chem. Eng. 9 (2021). https://doi.org/10.1016/j.jece.2021.105068.

[16] F. He, W. Jeon, W. Choi, Photocatalytic air purification mimicking the self-cleaning process of the atmosphere, Nat. Commun. 12 (2021) 10–13. https://doi.org/10.1038/s41467-021-22839-0.

[17] A. Talaiekhozani, S. Rezania, K.H. Kim, R. Sanaye, A.M. Amani, Recent advances in photocatalytic removal of organic and inorganic pollutants in air, J. Clean. Prod. 278 (2021) 123895. https://doi.org/10.1016/j.jclepro.2020.123895.

[18] C. Yang, G. Miao, Y. Pi, Q. Xia, J. Wu, Z. Li, J. Xiao, Abatement of various types of VOCs by adsorption/catalytic oxidation: A review, Chem. Eng. J. 370 (2019) 1128–1153. https://doi.org/10.1016/j.cej.2019.03.232.

[19] W. Zou, B. Gao, Y.S. Ok, L. Dong, Integrated adsorption and photocatalytic

degradation of volatile organic compounds (VOCs) using carbon-based nanocomposites: A critical review, Chemosphere. 218 (2019) 845–859. https://doi.org/10.1016/j.chemosphere.2018.11.175.

[20] C.T. Chekem, Y. Richardson, M. Drobek, G. Plantard, J. Blin, V. Goetz, Effective coupling of phenol adsorption and photodegradation at the surface of micro-and mesoporous TiO2-activated carbon materials, React. Kinet. Mech. Catal. 122 (2017) 1297–1321. https://doi.org/10.1007/s11144-017-1265-0.

[21] S. Ali, Z. Li, S. Chen, A. Zada, I. Khan, I. Khan, W. Ali, S. Shaheen, Y. Qu, L. Jing, Synthesis of activated carbon-supported TiO2-based nano-photocatalysts with well recycling for efficiently degrading high-concentration pollutants, Catal. Today. 335 (2019) 557–564. https://doi.org/10.1016/j.cattod.2019.03.044.

[22] V. Lekshmi Mohan, S.M. Shiva Nagendra, M.P. Maiya, Photocatalytic degradation of gaseous toluene using self-assembled air filter based on chitosan/activated carbon/TiO2, J. Environ. Chem. Eng. 7 (2019) 103455. https://doi.org/10.1016/j.jece.2019.103455.

[23] N.N. Bahrudin, Evaluation of degradation kinetic and photostability of immobilized TiO2/activated carbon bilayer photocatalyst for phenol removal, Appl. Surf. Sci. Adv. 7 (2022) 100208. https://doi.org/10.1016/j.apsadv.2021.100208.

[24] W.K. Jo, C.H. Yang, Granular-activated carbon adsorption followed by annular-type photocatalytic system for control of indoor aromatic compounds, Sep. Purif. Technol. 66 (2009) 438–442. https://doi.org/10.1016/j.seppur.2009.02.014.

[25] E. Hallemans, G. Coulbaux, M. Binet, C. Hort, L. Moynault, V. Hequet, Y. Andres, E. Hallemans, G. Coulbaux, M. Binet, C. Hort, V. Platel, CUBAIR , Confort des Usagers des Bâtiments tertiaires par l ’ usage de techniques de traitement de l ’ AIR To cite this version : HAL Id : hal-02363808, (2019).

[26] R. Jain, M. Mathur, S. Sikarwar, A. Mittal, Removal of the hazardous dye rhodamine B through photocatalytic and adsorption treatments, J. Environ. Manage. 85 (2007) 956–964. https://doi.org/10.1016/j.jenvman.2006.11.002.

[27] T.T. Lim, P.S. Yap, M. Srinivasan, A.G. Fane, TiO2/AC composites for

synergistic adsorption-photocatalysis processes: Present challenges and further developments for water treatment and reclamation, Crit. Rev. Environ. Sci. Technol. 41 (2011) 1173–1230. https://doi.org/10.1080/10643380903488664.

[28] A.H. Mamaghani, F. Haghighat, C.S. Lee, Photocatalytic degradation of VOCs on various commercial titanium dioxides: Impact of operating parameters on removal efficiency and by-products generation, Build. Environ. 138 (2018) 275–282. https://doi.org/10.1016/j.buildenv.2018.05.002.

[29] C. Andriantsiferana, E.F. Mohamed, H. Delmas, Sequential adsorption - Photocatalytic oxidation process for wastewater treatment using a composite material TiO2/activated carbon, Environ. Eng. Res. 20 (2015) 181–189. https://doi.org/10.4491/eer.2014.070.

[30] R. Chauveau, Modélisation multiparamètre du phénomène d ’ adsorption : détermination du temps de percée des cartouches de masques à gaz To cite this version : HAL Id : tel-01751295 soutenance et mis à disposition de l ’ ensemble de la Contact : ddoc-theses-contact@uni, (2018).

[31] B.C. Singer, A.T. Hodgson, H. Destaillats, T. Hotchi, K.L. Revzan, R.G. Sextro, Indoor sorption of surrogates for sarin and related nerve agents, Environ. Sci. Technol. 39 (2005) 3203–3214. https://doi.org/10.1021/es049144u.

[32] M. Spiandore, A. Piram, A. Lacoste, D. Josse, P. Doumenq, Hair analysis as a useful procedure for detection of vapour exposure to chemical warfare agents: Simulation of sulphur mustard with methyl salicylate, Drug Test. Anal. 6 (2014) 67–73. https://doi.org/10.1002/dta.1659.

[33] R.J. Feldman, Chemical agent simulant release from clothing following vapor exposure, Acad. Emerg. Med. 17 (2010) 221–224. https://doi.org/10.1111/j.1553-2712.2009.00650.x.

[34] G. Bikelytė, M.A.C. Härtel, T.M. Klapötke, B. Krumm, A. Sadaunykas, Experimental thermochemical data of CWA simulants: Triethyl phosphate, diethyl methylphosphonate, malathion and methyl salicylate, J. Chem. Thermodyn. 143 (2020). https://doi.org/10.1016/j.jct.2019.106043.

[35] S.L. Bartelt-Hunt, D.R.U. Knappe, M.A. Barlaz, A review of chemical warfare

agent simulants for the study of environmental behavior, Crit. Rev. Environ. Sci. Technol. 38 (2008) 112–136. https://doi.org/10.1080/10643380701643650.

[36] M. Grandcolas, T. Cottineau, A. Louvet, N. Keller, V. Keller, Solar light-activated photocatalytic degradation of gas phase diethylsulfide on WO3-modified TiO2 nanotubes, Appl. Catal. B Environ. 138–139 (2013) 128–140. https://doi.org/10.1016/j.apcatb.2013.02.041.

[37] A. Sengele, D. Robert, N. Keller, V. Keller, Modified-tio2 photocatalyst supported on β-sic foams for the elimination of gaseous diethyl sulfide as an analog for chemical warfare agent: Towards the development of a photoreactor prototype, Catalysts. 11 (2021). https://doi.org/10.3390/catal11030403.

[38] A. Sengele, D. Robert, N. Keller, V. Keller, A. Herissan, C. Colbeau-Justin, Ta-doped TiO2 as photocatalyst for UV-A activated elimination of chemical warfare agent simulant, J. Catal. 334 (2016) 129–141. https://doi.org/10.1016/j.jcat.2015.11.004.

[39] W. Abou Saoud, A. Kane, P. Le Cann, A. Gerard, L. Lamaa, L. Peruchon, C. Brochier, A. Bouzaza, D. Wolbert, A.A. Assadi, Innovative photocatalytic reactor for the degradation of VOCs and microorganism under simulated indoor air conditions: Cu-Ag/TiO2-based optical fibers at a pilot scale, Chem. Eng. J. 411 (2021) 128622. https://doi.org/10.1016/j.cej.2021.128622.

[40] M. Abidi, A. Hajjaji, A. Bouzaza, L. Lamaa, L. Peruchon, C. Brochier, S. Rtimi, D. Wolbert, B. Bessais, A. Amin Assadi, Modeling of indoor air treatment using an innovative photocatalytic luminous textile: reactor compactness and mass transfer enhancement, Chem. Eng. J. (2021) 132636. https://doi.org/10.1016/j.cej.2021.132636.

[41] Y. Serhane, A. Bouzaza, D. Wolbert, A.A. Assadi, New UV-LED frontal flow photocatalytic reactor for VOCs treatment: Compactness, intensification and optimization studies, Chem. Eng. J. 451 (2023) 138784. https://doi.org/10.1016/j.cej.2022.138784.

[42] P.A. Bourgeois, E. Puzenat, L. Peruchon, F. Simonet, D. Chevalier, E. Deflin, C. Brochier, C. Guillard, Characterization of a new photocatalytic textile for formaldehyde removal from indoor air, Appl. Catal. B Environ. 128 (2012) 171–178. https://doi.org/10.1016/j.apcatb.2012.03.033.

[43] C. Brochier, D. Malhomme, E. Deflin-Brevet « Nappe textile présentant des propriétés dépolluantes par photocatalyse» -no. de délivrance FR2910341, 2008-06-27 (A1) et FR2910341, 2009-02-06 (B1), 2007..

[44] C. Indermühle, E. Puzenat, F. Simonet, L. Peruchon, C. Brochier, C. Guillard, Modelling of UV optical ageing of optical fibre fabric coated with TiO2, Appl. Catal. B Environ. 182 (2016) 229–235. https://doi.org/10.1016/j.apcatb.2015.09.037.

[45] P. Danca, F. Bode, A. Meslem, C. Croitoru, M. Sandu, I. Nastase, C. Lungu, L. Batali, A. Correspondant, Experimental investigation of thermal vehicular environment during the summer season, n.d.

[46] R.M. Clark, Evaluating the Cost and Performance of Field-Scale Granular Activated Carbon Systems, Environ. Sci. Technol. 21 (1987) 573–580. https://doi.org/10.1021/es00160a008.

[47] W. Abou Saoud, A.A. Assadi, M. Guiza, A. Bouzaza, W. Aboussaoud, A. Ouederni, I. Soutrel, D. Wolbert, S. Rtimi, Study of synergetic effect, catalytic poisoning and regeneration using dielectric barrier discharge and photocatalysis in a continuous reactor: Abatement of pollutants in air mixture system, Appl. Catal. B Environ. 213 (2017) 53–61. https://doi.org/10.1016/j.apcatb.2017.05.012.

[48] D. Lancmuir, J.S. Herman, 1-S2.0-0016703780902264-Main, 44 (2002) 1–14. papers2://publication/uuid/5E9E5D34-242B-4117-8B39-BF4464A10B4B.

[49] R. Briner, D. Chevillat, S. Neff, M. Scheen, Complémentaire Dans Le Traitement De L ' Épilepsie ?, 33 (2013) 1–41.

[50] V.E. Malheureusement, ergonomie Débit ventilatoire de travail, (1998) 343–350.

[51] M. Malayeri, F. Haghighat, C.S. Lee, Kinetic modeling of the photocatalytic degradation of methyl ethyl ketone in air for a continuous-flow reactor, Chem. Eng. J. 404 (2021) 126602. https://doi.org/10.1016/j.cej.2020.126602.

[52] G. Zhang, Y. Liu, Z. Hashisho, Z. Sun, S. Zheng, L. Zhong, Adsorption and photocatalytic degradation performances of TiO2/diatomite composite for volatile organic compounds: Effects of key parameters, Appl. Surf. Sci. 525

(2020). https://doi.org/10.1016/j.apsusc.2020.146633.

[53] J. Chen, G. Li, Z. He, T. An, Adsorption and degradation of model volatile organic compounds by a combined titania-montmorillonite-silica photocatalyst, J. Hazard. Mater. 190 (2011) 416–423. https://doi.org/10.1016/j.jhazmat.2011.03.064.

[54] A.M. Vandenbroucke, R. Morent, N. De Geyter, C. Leys, Non-thermal plasmas for non-catalytic and catalytic VOC abatement, J. Hazard. Mater. 195 (2011) 30–54. https://doi.org/10.1016/j.jhazmat.2011.08.060.

[55] T. Martinez, A. Bertron, G. Escadeillas, E. Ringot, V. Simon, BTEX abatement by photocatalytic TiO2-bearing coatings applied tocement mortars, Build. Environ. 71 (2014) 186–192. https://doi.org/10.1016/j.buildenv.2013.10.004.

[56] B. Boulinguiez. Procédé d'adsorption et régénération électrothermique sur textile de carbone activé - Une solution pour la problématique des COV dans des gaz à fort potentiel énergétique. (2010). https://theses.hal.science/tel-00540206.

[57] W. Abou Saoud, A.A. Assadi, A. Kane, A.V. Jung, P. Le Cann, A. Gerard, F. Bazantay, A. Bouzaza, D. Wolbert, Integrated process for the removal of indoor VOCs from food industry manufacturing: Elimination of Butane-2,3-dione and Heptan-2-one by cold plasma-photocatalysis combination, J. Photochem. Photobiol. A Chem. 386 (2020) 112071. https://doi.org/10.1016/j.jphotochem.2019.112071.

[58] S. Deepracha, A. Ayral, M. Ogawa, Acceleration of the photocatalytic degradation of organics by in-situ removal of the products of degradation, Appl. Catal. B Environ. 284 (2021). https://doi.org/10.1016/j.apcatb.2020.119705.

[59] M. Dell'Edera, C. Lo Porto, I. De Pasquale, F. Petronella, M.L. Curri, A. Agostiano, R. Comparelli, Photocatalytic TiO2-based coatings for environmental applications, Catal. Today. 380 (2021) 62–83. https://doi.org/10.1016/j.cattod.2021.04.023.

[60] A. Sengele, Décontamination et dépollution par photocatalyse : réalisation d ' un dispositif d ' élimination d ' agents chimiques toxiques et de polluants dans l ' air et dans l ' eau Armelle Sengele To cite this version : HAL Id : tel-01304774,

(2016).

[61] Z. Aslam, I.A. Hussein, R.A. Shawabkeh, M.A. Parvez, W. Ahmad, Ihsanullah, Adsorption kinetics and modeling of H2S by treated waste oil fly ash, J. Air Waste Manag. Assoc. 69 (2019) 246–257. https://doi.org/10.1080/10962247.2018.1536004.

[62] S. Kamravaei, P. Shariaty, M. Jahandar Lashaki, J.D. Atkinson, Z. Hashisho, J.H. Phillips, J.E. Anderson, M. Nichols, Effect of Beaded Activated Carbon Fluidization on Adsorption of Volatile Organic Compounds, Ind. Eng. Chem. Res. 56 (2017) 1297–1305. https://doi.org/10.1021/acs.iecr.6b04165.

[63] S.K. Kam, M.G. Lee, Adsorption characteristics of antibiotics amoxicillin in aqueous solution with activated carbon prepared from waste citrus peel, Appl. Chem. Eng. 29 (2018) 369–375. https://doi.org/10.14478/ace.2018.1015.

[64] W. Abou Saoud, A.A. Assadi, M. Guiza, A. Bouzaza, W. Aboussaoud, I. Soutrel, A. Ouederni, D. Wolbert, S. Rtimi, Abatement of ammonia and butyraldehyde under non-thermal plasma and photocatalysis: Oxidation processes for the removal of mixture pollutants at pilot scale, Chem. Eng. J. 344 (2018) 165–172. https://doi.org/10.1016/j.cej.2018.03.068.

[65] T. Zadi, M. Azizi, N. Nasrallah, A. Bouzaza, R. Maachi, D. Wolbert, S. Rtimi, A.A. Assadi, Indoor air treatment of refrigerated food chambers with synergetic association between cold plasma and photocatalysis: Process performance and photocatalytic poisoning, Chem. Eng. J. 382 (2020) 122951. https://doi.org/10.1016/j.cej.2019.122951.

[66] A.A. Assadi, J. Palau, A. Bouzaza, D. Wolbert, Modeling of a continuous photocatalytic reactor for isovaleraldehyde oxidation: Effect of different operating parameters and chemical degradation pathway, Chem. Eng. Res. Des. 91 (2013) 1307–1316. https://doi.org/10.1016/j.cherd.2013.02.020.

[67] D.T. Tefera, Z. Hashisho, J.H. Philips, J.E. Anderson, M. Nichols, Modeling competitive adsorption of mixtures of volatile organic compounds in a fixed-bed of beaded activated carbon, Environ. Sci. Technol. 48 (2014) 5108–5117. https://doi.org/10.1021/es404667f.

[68] W.K. Pui, R. Yusoff, M.K. Aroua, A review on activated carbon adsorption for

volatile organic compounds (VOCs), Rev. Chem. Eng. 35 (2019) 649–668. https://doi.org/10.1515/revce-2017-0057.

[69] Z. Aslam, I.A. Hussein, R.A. Shawabkeh, M.A. Parvez, W. Ahmad, Ihsanullah, Adsorption kinetics and modeling of H2S by treated waste oil fly ash, J. Air Waste Manag. Assoc. 69 (2019) 246–257. https://doi.org/10.1080/10962247.2018.1536004.

[70] Y. Serhane, N. Belkessa, A. Bouzaza, D. Wolbert, A.A. Assadi, Continuous air purification by front flow photocatalytic reactor: Modelling of the influence of mass transfer step under simulated real conditions, Chemosphere. 295 (2022) 133809. https://doi.org/10.1016/j.chemosphere.2022.133809.

[71] A.A. Assadi, B. Abdelkrim, W. Dominique, Kinetic Modeling of VOC Photocatalytic Degradation Using a Process at Different Reactor Configurations and Scales, Int. J. Chem. React. Eng. 14 (2016) 395–405. https://doi.org/10.1515/ijcre-2015-0003.

[72] A.A. Assadi, A. Bouzaza, D. Wolbert, Photocatalytic oxidation of trimethylamine and isovaleraldehyde in an annular reactor: Influence of the mass transfer and the relative humidity, J. Photochem. Photobiol. A Chem. 236 (2012) 61–69. https://doi.org/10.1016/j.jphotochem.2012.03.020.

[73] S. Bourassa, Impact sur le travail respiratoire et les échanges gazeux pour l ' utilisateur d ' un masque à gaz Impact sur le travail respiratoire et les échanges gazeux pour l ' utilisateur d'un masque à gaz, (2017). corpus.ulaval.ca